(Received 16 November 2024, Accepted 31 December 2024, Scheduled 26 January 2025)

Design of Metamaterial Absorber Independent in Incident Angle for Solar Cell Applications

Asmaa S. Mohammed[1], Ayad Shohdy[2], Shazly A. Mohammed[3], and Ahmed M. Montaser[1,*]

[1]*Faculty of Technology and Education, Sohag University, Sohag, Egypt*
[2]*Faculty of Engineering, Sohag University, Sohag, Egypt*
[3]*Faculty of Engineering, South Valley University, Qena, Egypt*

ABSTRACT: This study proposes designing and developing a metamaterial absorber that improves the efficiency of solar cells. The design includes circular forms with rectangle gaps etched on the upper surface of an FR4 substrate, with a copper sheet serving as an isolating substrate for the ground beneath. The structure operates in the tera frequency ranges to accommodate all infrared wavelengths of the sun's spectrum. Furthermore, the constructed metamaterial unit cell is used to build a metamaterial array absorber, which increases the rate of energy harvest from the sun spectrum. The two designs showed absorption rates of approximately 96.75% and 99.85% at 94.85 THz and 109.08 THz resonant frequencies, respectively. In addition, a top surface of microwave cross-polarization conversion (CPC) is also generated and simulated. The structure of the proposed microwave unit cell consists of the same metamaterial absorber design. Efficient cross-conversion is achieved across a wide frequency band (9 GHz to 15 GHz), with polarization conversion effectiveness exceeding 99%. The suggested CPC design has three resonance bands with 50% fractional bandwidth (FBW) and achieves a stable polarization response at oblique incidence angles up to 35°.

1. INTRODUCTION

Fossil-fuel (conventional) energy sources, such as petroleum and coal, according to the 2014 Global Energy Statistic Report, account for 87% of all global energy use [1]. This high percentage seriously harms ecosystems in addition to making the production of fossil fuels challenging. Finding a substitute for clean, constant, relishable, and refillable energy sources is therefore essential. Solar radiation constitutes one of the greatest efficient sources of clean, renewable energy producing light, heat, lighting, and other sorts of energy [2–4]. Solar cells, commonly known as photovoltaic panels, generate electricity from solar energy. Solar cells are typically built of silicon, a material which comes into contact with photons of sunlight inside the cell, forcing atoms to lose their electrons from the material known as semiconductors and form electrical gaps that produce energy [5, 6]. The primary benefit of any photovoltaic panel-based structure is its ability to operate without the requirement for battery replacement on occasion. Nevertheless, these kinds of cells are able to absorb specific frequency bands of solar light, which give an efficiency of 30%. The electrical band gap prevents the solar cells from turning all solar light into electricity, is the cause of this low efficiency [7].

A recently discovered method based on the metamaterials methodology is utilized to improve the design of solar cells. New synthetic materials known as "metamaterials" are created with specific qualities not found in nature. Because of their intelligent properties, metamaterials are structured in periodic patterns on scales lesser than the spectral range of the processes they affect. They can process electromagnetic (EM) waves [8], preventing, absorbing, and bending EM waves [9–11]. They also have negative refract properties [12], which allow them to serve as ultra-lenses [13]. These metamaterial absorbers replace the photovoltaic solar cells to overcome its main disadvantages [14]. The key idea behind this technique is to scale and operate the absorbers at extremely high frequencies (THz), i.e., very short wavelength in the infrared regime. The concept of collecting solar energy from sun and earth radiation using metamaterial absorber is based on the fact that when an EM wave is incident to an absorber, a time varying current will be induced, and thus, a voltage will be generated at the feeding point of the absorber [15, 16]. This induced current or generated voltage will oscillate at the frequency of the incident wave. Hence, in order to obtain DC power, a suitable rectifier circuit should be embedded at the feed point of absorber. This type of energy harvesting systems are called rectennas and consist of antennas connected to a rectifier that converts the received signal to DC power and produce electricity. The metamaterial absorber shows a wider angular reception characteristic than that of photovoltaic devices. This optimizes the solar energy collection during day and cancels the need for sun tracking systems [14].

According to literature reports, metamaterials absorbers have been the subject of numerous study projects and inquiries by various scholars, where metamaterial absorbers are expressed in a wide variety of ways [17–19]. An infinite number of multi-resonance nanoscale particles are incorporated into the design of a metamaterials-based absorber presented in [20].

* Corresponding author: Ahmed Mohamed Montaser (Ahmed.Montaser1@techedu.sohag.edu.eg).

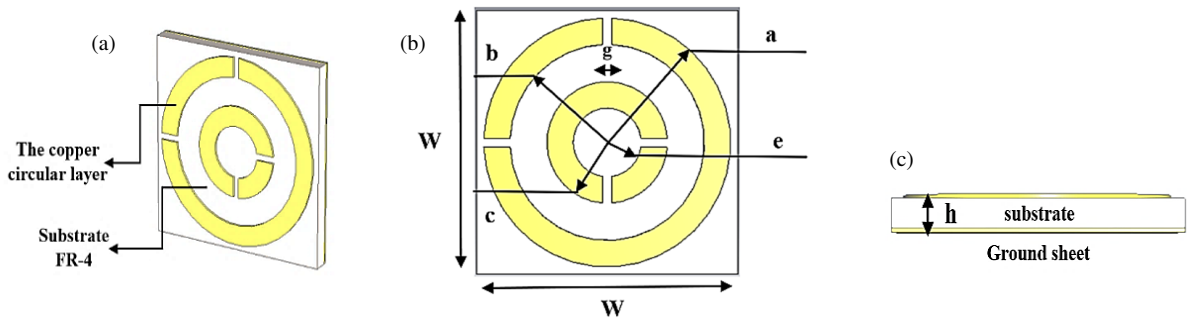

FIGURE 1. Proposed design of absorber unit cell. (a) 3-D view, (b) 2-D front view, (c) side view.

Significant solar energy absorption is possible thanks to the absorber. A brand-new type of metamaterial absorption in many frequency ranges is created, described, and studied in [5]. The metamaterial-based design is especially offered in the whole range of the solar radiation to maximize solar energy utilization. Visible and infrared spectrum are optimally absorbed by the developed metamaterial-based solar cells. Furthermore, several unique and unconventional concepts for expanding antenna arrays and metamaterial properties in most kinds of antennae and material have been offered [21–24]. One of these tactics was utilized to improve the features of the suggested metamaterial antenna arrays by executing a parameter sweeps on the most important and effective factors that determine the meta-antenna array's attributes, such as the rate of absorption. Furthermore, a structure made of super-absorbing material was constructed to collect sunlight, with rates of absorption approaching 99% [25].

Many fascinating occurrences are naturally sensitive to polarization states. They have traditionally been one of the most important properties of EM waves, thus substantial efforts have been undertaken to control and manage them [26–29]. Metamaterials, particularly planar metamaterials, have recently gained a lot of attention due to their unusual features. It has a verity of applications including planar optics [30], anomalous refraction [31], angular momentum of light [32], optical vortex creation [33], cross polarization conversion (CPC) [34], transmission and reflection surface types [35–38]. Because many phenomena are polarization delicate, a large portion of metasurface research focuses on surface that can govern and change the polarization of EM radiation. Traditional processes such as crystal optical reflection and Faraday operation can be used to change the polarization of electromagnetic radiation, but they require a lot of space and are only effective for a short bandwidth [39]. As a result, EM polarization states can be freely controlled and modified utilizing sub-wavelength metamaterials. Note that two-dimensional metamaterials, known as metasurfaces, are used to create high-performance polarization converters [30]. Polarization conversions can be achieved over many frequency bands of EM spectrum using various component shapes, such as plasmon nano-rods in the visual system [40], circular divided rings in the infrared [41], metal-based grating at terahertz [42], self-complementary rings [43], rectangle loops with opposite microstrips [44], and double-head-arrow form [45] in the microwave system [46].

This study proposes and presents a novel absorber structure based on metamaterial technologies to increase the effectiveness of solar cells. A basic structural unit cell made up of two distinct layers with rectangle gaps of constant size may absorb a large amount of infrared at different tera hertz. Furthermore, this unit cell is utilized to create arrays of varied sizes with the same infrared resonant rate in order to absorb as many photons that are available in the spectrum of the sun. To validate the metamaterial results, a proposed wide-band and electrically thin CPC metasurface is modified to operate at microwave frequencies, where a high polarization conversion ratio (PCR) is achieved and fully independent of incident wave polarization. Furthermore, the proposed upper surface exhibits a consistent reaction to changes in incident angle. Because of the sub-wavelength unit cell dimension's thin dielectric thickness and overall optimal design, the metasurface interaction is independent of the incident wave's incidence angle, making it a viable contender for a wide range of applications. Furthermore, numerical analysis of polarization states is offered across the whole spectrum. The simulation is handled by the CST-microwave studio (CST-MWS) software simulator.

2. DESIGN AND ANALYSIS

2.1. Design of the Proposed Metamaterial Unit Cell in the Infrared Band

The suggested layout for the unit cell design includes printed circular forms with rectangle gaps on the upper surface of the substrate layer, accompanied by a sheet of copper serving as the base. As depicted in Fig. 1, the suggested unit cell's architecture is derived from earlier research and analysis that is documented in the literature [3–9]. The reference form and general idea were inspired by [39, 47]. The optimum parameters for the unit cell design are indicated in Table 1. The reference's shape is modified to make it simpler, more compact, and capable of dual-band operation. The parameter extensive evaluations are performed on the proposed unit cell to ensure that it works properly in the intended range of frequencies. This approach combines two different pieces into a unit cell. One of the two separate fragments has a negative relative permeability, whereas the other has a negative relative permittivity. The technique is based on the premise that resonance-sensitive materials show high levels of effective magnetism near resonance when being subjected to an axial forces magnet, with substantially higher values in the narrow range below the rings' quasi-static reso-

TABLE 1. Geometrical parameters of the suggested infrared absorption unit cell and CPC metasurface.

Parameters	infrared unit cell	CPC metasurface	Description
	Value (μm)	Value (mm)	
w	3	5	The substrate material's width
h	0.24	2.4	thickness of the substrate material
g	0.1	0.25	rectangular gap width
a	1.41	2	the outer radius of the outer slice
b	1.11	1.5	the inner radius of the outer slice
c	0.68	1	the outer radius of the entire slice
e	0.38	0.5	the inner radius of the entire slice

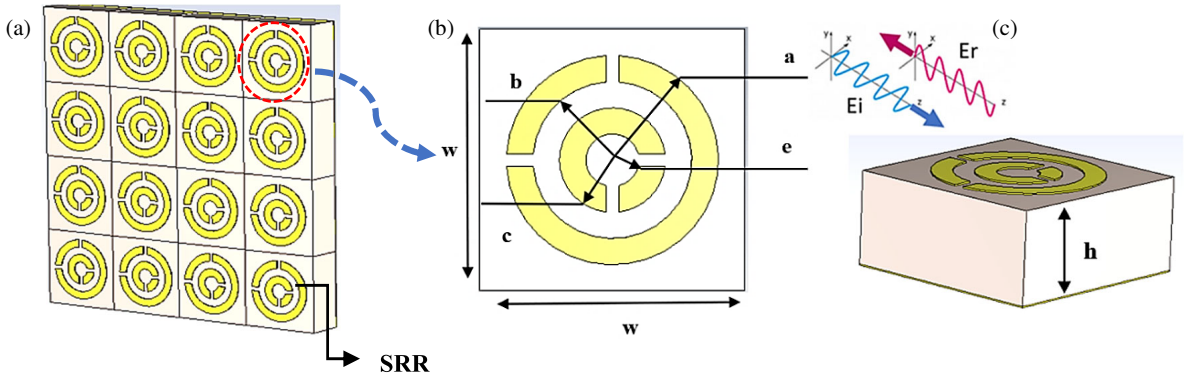

FIGURE 2. (a) A general schematic depiction of the proposed CPC metasurface, (b) top view of the unit cell, (c) 3D view.

nant frequency and highly negative results in the narrow region above [48].

The structure's lower foundation layer is a copper sheet with 0% transfer, measuring 3×3 μm in infrared, then follows a layer of insulation that serves as the substrate. The FR-4 substrate has a 0.24 μm thickness, a permittivity ratio of 4.4, and a tangent loss of 0.025. Two copper circular shapes with a spacing of 0.1 μm are printed atop the substrate surface. Copper sheet has an electric conductivity of 5.8×10^7 S/m, thermal conductivity of 401 w/K/m, and thickness of 0.0035 μm.

The solar cells' absorption rate $A(\text{ɯ})$ can be computed using [5]:

$$(\text{ɯ}) = 1 - R(\text{ɯ}) - T(\text{ɯ}) \quad (1)$$

where $(\text{ɯ}) = |S_{11}|^2$ and $T(\text{ɯ}) = |S_{21}|^2$ are the reflectivity and transmission at a specific frequency range, respectively. Throughout the current work, there will be not a single transmission to be calculated ($T(\text{ɯ}) \to 0$), because it is obstructed by the continuous copper sheet. As a consequence, only the reflection must be investigated. Therefore, the absorption rate is changed to be computed as follows:

$$(\text{ɯ}) = 1 - R(\text{ɯ}) \quad (2)$$

The reflectance can be stated as follows:

$$R(\text{ɯ}) = \frac{\text{Reflected power at port 1}}{\text{Incident power on port 1}} \quad (3)$$

As the amount of reflection decreases, the absorption rate rises and approaches unity, which is the major purpose of this research. This is demonstrated via the use of a metamaterial absorber.

2.2. Geometric Configuration of the CPC Metasurface Unit Cell

The infrared metamaterial unit cell is modified to CPC metasurface to operate at microwave frequencies. Fig. 2 shows an illustration of the planned CPC metasurface unit cell. The unit cell consists of two metal sheets separated by a 2.4 mm thickness FR4 material with a dielectric constant $\varepsilon_r = 4.4$ and tangent to loss $\tan\delta = 0.025$. The top metallic layer is made up of printed circular forms with rectangular gaps on the substrate's top surface, which is supported by a copper ground plate. The metallic layers are composed of copper material with a conductivity of 5.8×10^7 S/m and a thickness of 35 microns. Fig. 2(a) shows the two-dimensional periodic arrays of metallic coupled split ring resonators (SRRs) arranged on top of the dielectric, which is supported by a metallic plane. The designed unit cell is given in Fig. 2(b), and the optimum parameters for the proposed CPC metasurface unit cell are also indicated in Table 1 for comparison. Fig. 2(c) shows a three-dimensional schematic depiction of the proposed unit cell.

Jones transmission and reflection matrices serve to characterize the theory of polarization conversion. Transmission is completely nonexistent in a reflector design, thus only incident and reflected fields are taken into account. The wave polarization is characterized in terms of its orthogonal parts, and the degree of polarization conversion is calculated through contrasting the co- and cross-components of the incoming and re-

flected fields. The anisotropy shape of the unit cell interacts differently with the two perpendicular components, resulting in cross-conversion. Consider a vertically polarized incoming wave that propagates along the positive z axis and strikes a metasurface reflection at its normal incidence. Equation (4) represents the wave's electric field vector [47].

$$\overrightarrow{E^i} = \left|\overrightarrow{E_x^i}\right| e^{-j\varphi_{xi}} \vec{e}_y \tag{4}$$

Superscript i represents the incident field, and subscript y denotes the vector's component label. φ_i represents the directional angle of the field's phasor. $\vec{e}_y$ represents the unit vector in the y direction. The electrical field vectors can rotate in the x-y plane following reflection from the contact; therefore, both orthogonal components, as shown in Equation (5a), are necessary for a complete description of the reflected wave. Equation (5b) expresses these component fields in terms of complex reflection coefficients.

$$\overrightarrow{E^r} = \left|\overrightarrow{E_x^r}\right| e^{-j\varphi_x} \vec{e}_x + \left|\overrightarrow{E_y^r}\right| e^{-j\varphi_x} \vec{e}_y \tag{5a}$$

$$\overrightarrow{E^r} = \left|\overrightarrow{E_y^i}\right| \left(R_{xy} e^{-j\varphi_x} \vec{e}_x + R_{yy} e^{-j\varphi_y} \vec{e}_y\right) \tag{5b}$$

In the equations, superscript r indicates the mirrored field, and subscripts x and y indicate field constituent labels. The Jones reflection matrix, illustrated in Equation (6), shows the overall connection between the linearly polarized incident and reflected fields.

$$\begin{bmatrix} E_{xr} \\ E_{yr} \end{bmatrix} = \begin{bmatrix} R_{xx} & R_{xy} \\ R_{yx} & R_{yy} \end{bmatrix} \begin{bmatrix} E_{xi} \\ E_{yi} \end{bmatrix} = R_{lin} \begin{bmatrix} E_{xi} \\ E_{yi} \end{bmatrix} \tag{6}$$

R_{lin} is also referred to as the Jones Reflection Matrix, and it describes the wave reflection phenomena for polarized linear waves. The co-polarization coefficients of reflection R_{xx} and R_{yy} can be defined as the ratio of the values of horizontally reflected with horizontal incidence fields ($R_{xx} = |E_{xr}|/|E_{xi}|$) and vertically reflected to vertical incidence ($R_{yy} = |E_{yr}|/|E_{yi}|$). In a similar vein, R_{xy} and R_{yx} are cross-polarization coefficients that link the cross-field components, i.e., ($R_{xy} = |E_{xr}|/|E_{yi}|$) and ($R_{yx} = |E_{yr}|/|E_{xi}|$).

3. RESULTS AND DISCUSSION

3.1. Results and Discussion of the Proposed Metamaterial Unit Cell in the Infrared Band

The suggested construction is modelled using the computer simulation technology microwave studio (CST-MWS) simulator. The proposed structure exhibits two peaks of absorption at two resonance frequencies. Absorption peaks of 96.75% and 99.85% at 94.85 THz and 109.08 THz frequencies respectively are shown in Fig. 3, where $A(\omega)$ is the absorption rate and S_{11} is the reflection coefficient.

By examining distributions of the electric field and surface current at resonance frequencies as presented in Figs. 4 and 5,

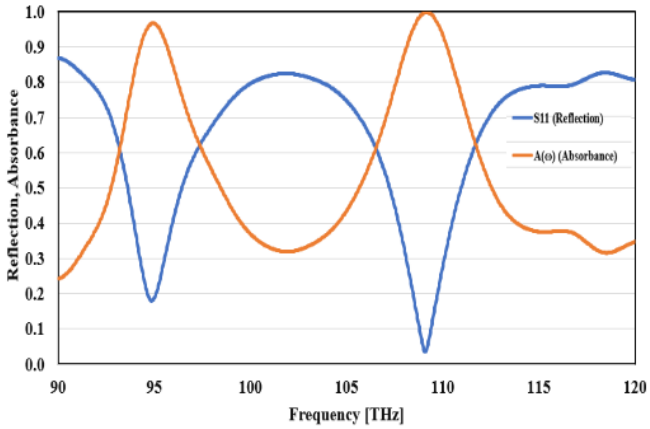

FIGURE 3. Simulated reflection and absorption rate of the designed absorber unit cell at the infrared radiation.

the figures validate the physical process underlying the operation of a metamaterial-based solar cell absorber at resonance. At the resonance frequencies of 94.85 THz and 109.08 THz, Fig. 4 depicts the electric field distribution throughout the cell. It is observed that the intensity of the electric field is focused in the outer and inner circular slices of the circuit, as well as the chip's side rectangular gaps at the two frequencies. Fig. 5 depicts the surface current distribution at both resonance frequencies. As seen in the figure, the current spreads broadly across the entire circle form at the resonant frequency of 94.85 THz, whereas the outer and inner circular shapes have the same current distribution at the other resonant frequency of 109.08 THz but are much denser.

Figure 6 depicts the configuration and construction of a unit cell array, which is designed to gather and absorb as much solar infrared radiation as possible. It also displays the simulation results for this matrix's absorption and reflection coefficients. Based on the data supplied, it is obvious that the absorption rate and high performance of the unit cell remain constant.

3.2. Results and Discussion of the CPC Metasurface

3.2.1. Absorption and Reflection Results

The reflection and absorbance results in microwave range are shown in Fig. 7. Fig. 8(a) shows the magnitudes of the co- and cross-polarization coefficients of reflection with normal conditions for both x- and y-polarized incident waveforms. Fig. 8(a) clearly indicates that the co-polarization coefficients of reflection R_{yy} and R_{xx} are less than -10 dB, whereas the cross-polarization reflection coefficient R_{xy} and R_{yx} are greater than -1 dB over a wide frequency band (9 GHz to 15 GHz). Fig. 8(a) also displays three plasmonic resonances at 9.76 GHz, 11.39 GHz, and 13.77 GHz, with co-polarization reflection coefficients of -30.46 dB, -35.76 dB, and -35 dB, respectively. At these resonant frequencies, the cross-polarization coefficient of reflection is nearly 0 decibels. To determine the efficacy of polarization conversion, we employ an indicator known as PCR, which is defined as PCR $= |R_{xy}|^2/(|R_{xy}|^2 + |R_{yy}|^2)$. It is a power ratio between the reflected cross-polarization component and the total reflected power. For flawless cross con-

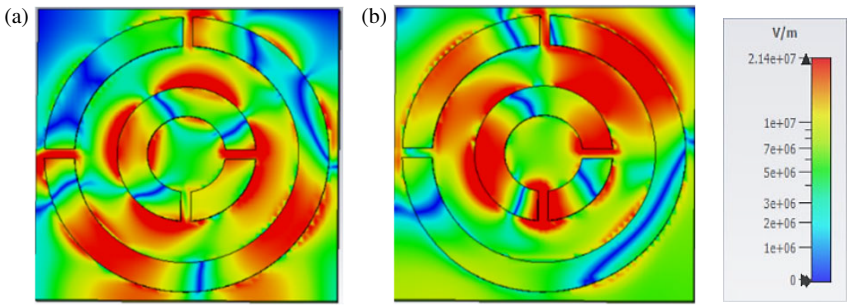

FIGURE 4. Distribution of the unit cell's electric field at (a) 94.85 THz frequency, (b) 109.08 THz frequency.

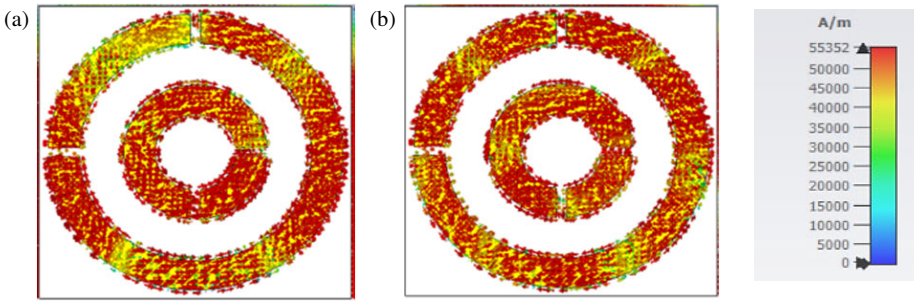

FIGURE 5. Distribution of the unit cell's surface current at (a) 94.85 THz frequency, (b) 109.08 THz frequency.

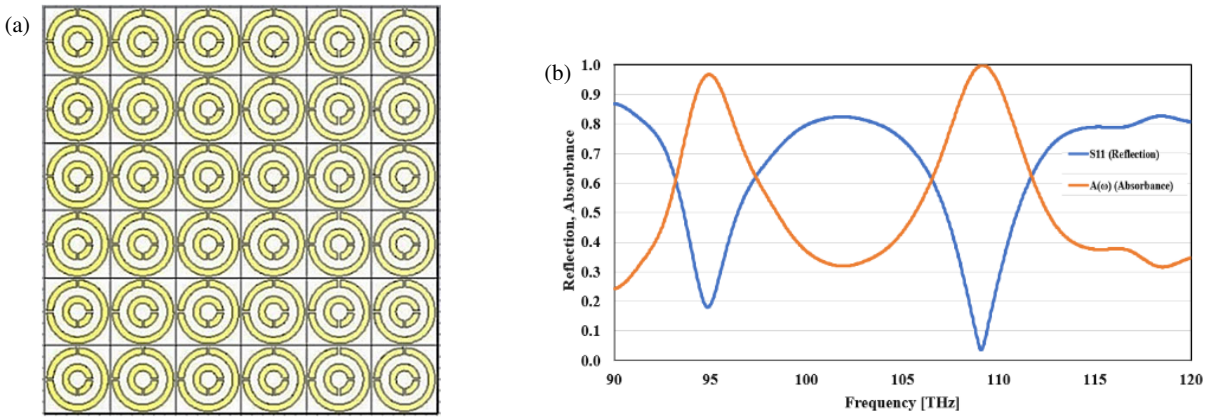

FIGURE 6. (a) The configuration of a unit cell array. (b) Simulated reflection and absorption rate of unit cell array.

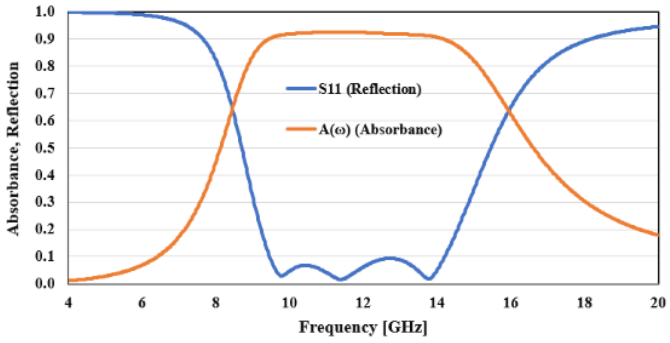

FIGURE 7. The absorbance and reflection results in microwave range.

version, use PCR = 1 or conversion efficiency = 100%. Fig. 8(b) shows the PCR of the suggested metasurface for normal incidence. At all three resonances (9.76 GHz, 11.39 GHz, and 13.77 GHz), a nearly ideal polarization conversion ratio of 100% is attained, and the efficiency is more than 90% across a large frequency range (9 GHz to 15 GHz).

3.2.2. Angular Stability

The performance of the proposed absorber is studied at different incident angles. Fig. 9 shows the simulated reflection and absorbance results in microwave range at different incident angles, when the angle is varied from 0° to 35°. In order for the CPC metasurface be useful in a wide range of applications, the metasurface's reaction must be consistent enough to resist variations in angle of incident. The angle stability of the metasurface is frequently proportional to the substrate thickness and dielectric constant. Metasurfaces with thin insulating substrates exhibit higher angular stability. The thiner the metasurface is

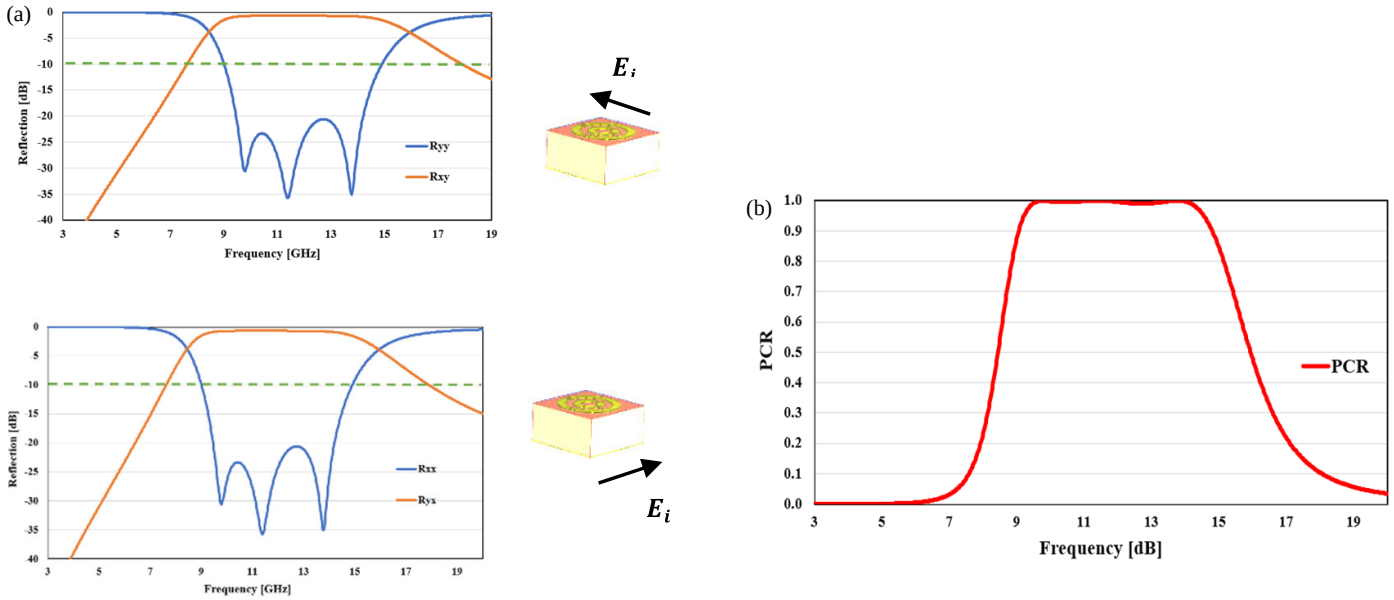

FIGURE 8. (a) The magnitude of cross- and co-polarized reflection coefficients for both x- and y-polarized incident waves, (b) PCR.

TABLE 2. Comparison with other cross-polarization conversion metasurface related works.

Design	Substrate with thickness (electrical size)	Operating bandwidth (GHz)	PCR	Fractional bandwidth (FBW) (%)	Angular stability
Ref. [29]	FR4 $0.05\lambda_o$	9.24–17.64	90%	62.5%	Only for normal incidence wave.
Ref. [38]	F4B-2 $0.06\lambda_o$	9.1–12.9	99%	34.5%	Only for normal incidence wave.
Ref. [39]	FR4 $0.04\lambda_o$	5–10.8	60%	73%	Angularly stable up-to 45°.
Ref. [46]	F4B $0.067\lambda_o$	14.2–36	90%	86.9%	Angularly stable up-to 20° b/w 14–27 GHz only.
Ref. [47]	FR4 $0.048\lambda_o$	8–18.5	90%	80%	Angularly stable up-to 45°.
Present Study	FR4 $0.096\lambda_o$	9–15	99%	50%	Angularly stable up-to 35°.

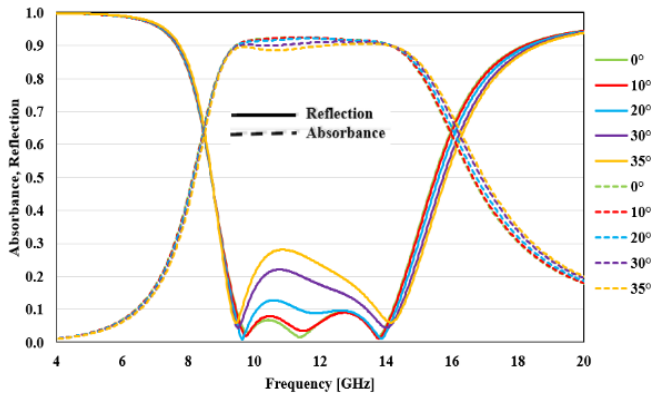

FIGURE 9. Simulated reflection and absorbance results in microwave range at different incident angles.

with respect to the incoming wavelength, the more consistent its response is to variations in the angle of incident; nevertheless, the band width will be smaller. Another approach to achieve stability in angles is to use a material with a large dielectric constant, which reduces bandwidth. Angular stability, bandwidth, and metasurface thickness are often trade-off. A potential way for achieving both wide bandwidth and angular stability is to carefully design the metal framework on top of the insulator so that the unit cell can experience several resonant frequencies. Figure 10 depicts the co- and cross-polarized coefficients of reflection at different incidence angles. Figs. 10(a) and 10(b) show the co- and cross-polarized coefficients of reflection at various angles of incident when the reflected wave is x-polarized. Fig. 10(b) shows that the cross-polarized coefficient of reflection remains essentially constant as the angle of incident changes. The minor divergence in the cross-polarized coefficient of reflection for the x-polarized case at large angles of incident is due to an electrical field component entering the SRR loop and disrupting current flow. Figs. 10(c) and 10(d) depict the co- and cross-polarized coefficients of reflection when the incident waveform is y-polarized at varying incident angles.

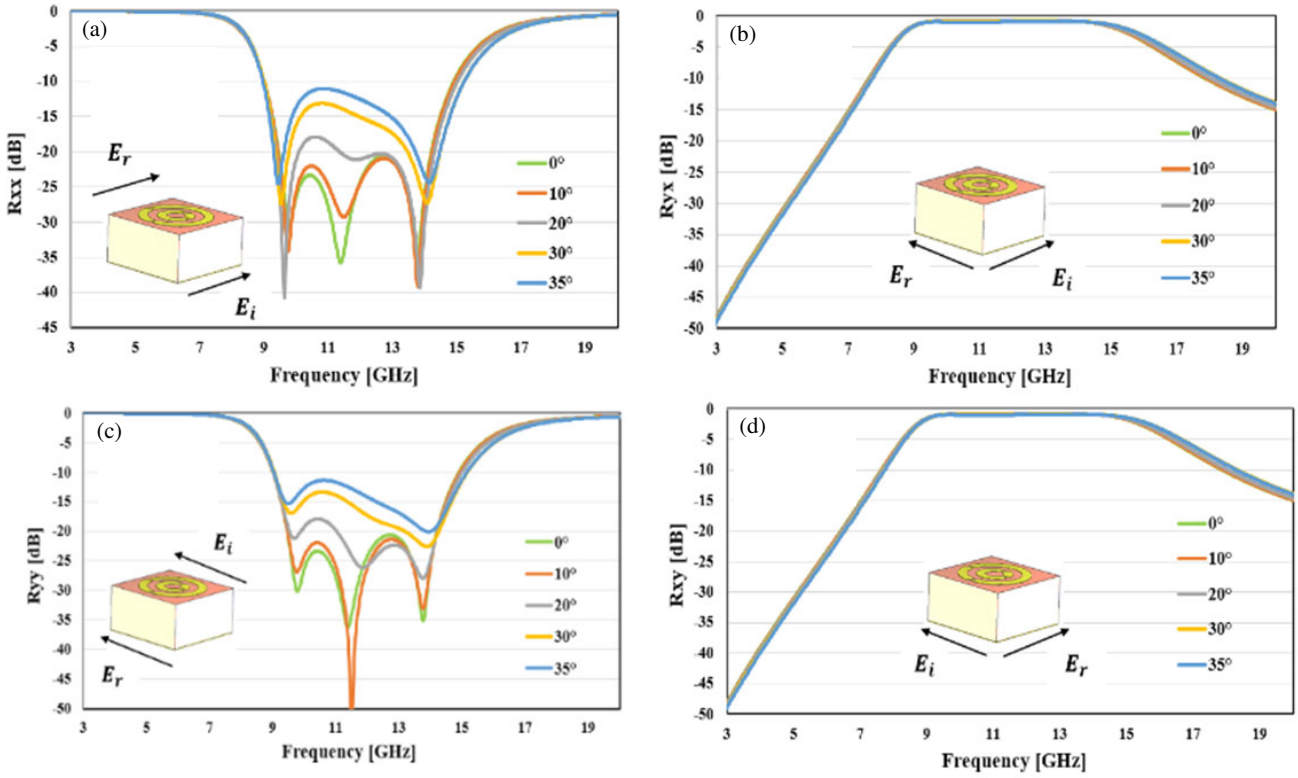

FIGURE 10. (a) Co-polarized, (b) cross-polarized reflection coefficients for x-polarized incident wave, (c) co-polarized, (d) cross-polarized reflection coefficient for the y-polarized incident wave.

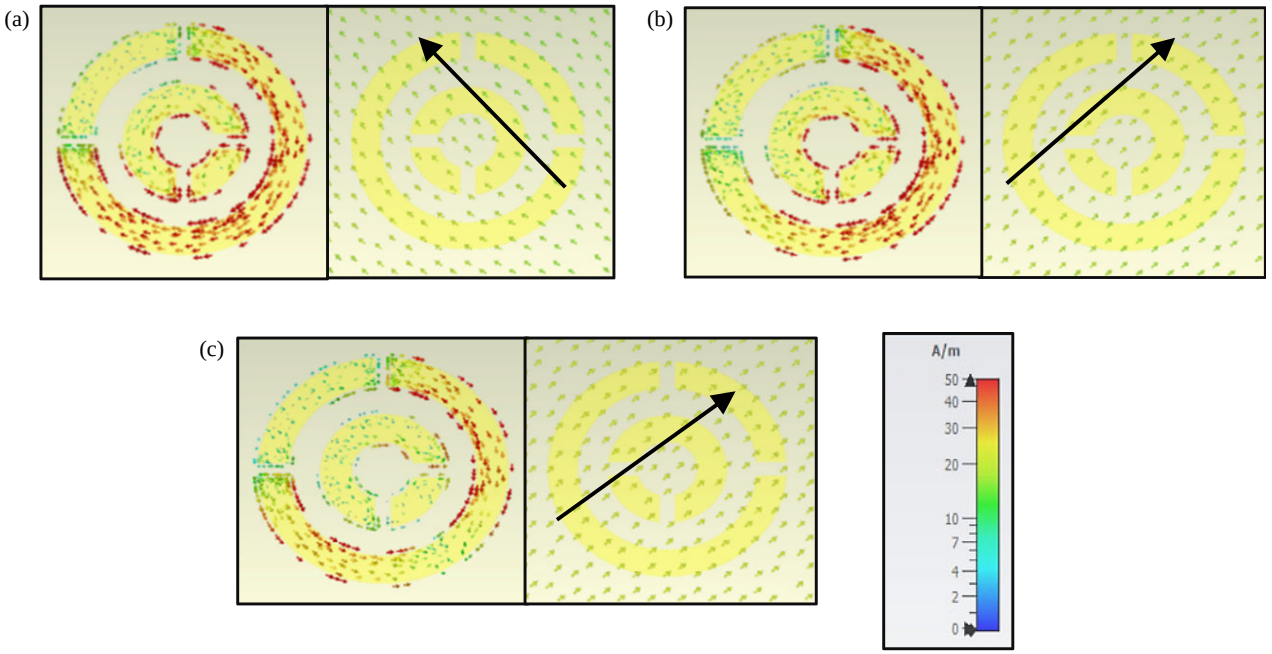

FIGURE 11. Surface current distributions on the top and back plane at three distinct resonance frequencies, (a) 9.76 GHz, (b) 11.39 GHz, (c) 13.77 GHz.

The suggested design, as illustrated in Fig. 10(d), yields a constant cross-polarized coefficient of reflection even when incident waves are y-polarized. The modest deviation in the cross-polarized coefficient of reflection for the y-polarized case at large angles of incidence is due to the field of magnets, which enters the SRR loop and induces current in the SRR.

3.2.3. Analysis Based on Surface Current

The physical process of CPC is studied utilizing the surface current distribution on the metasurface architecture and the base plane of the unit cell. Figs. 11(a), (b), (c) illustrate the current distributions at three resonant frequencies (9.76 GHz, 11.39 GHz, and 13.77 GHz) on the upper layer (pattern plane) and the back plane (ground), respectively. The current is densely distributed across the cell's internal and external circuits at resonant frequencies 9.76 GHz and 11.39 GHz, as shown in Figs. 11(a), (b), but less densely at resonance frequency 13.77 GHz, as provided in Fig. 11(c).

Table 2 presents a performance assessment of the proposed design against other recent related works. It is observed that the proposed design has much more angular stability than other cross-conversion systems. The designs of [47] and [39] have 45° angular stability, but their polarization conversion efficiency is substantially lower than the proposed design. Ref. [38] has good polarization efficiency, but it is severely hampered by a low fractional bandwidth (FBW). As a result, the current study delivers outstanding polarization efficiency and angular stability.

4. CONCLUSION

A metamaterial technique is presented to create a dual-band solar infrared absorber. The suggested design consists of two circular forms etched with rectangle gaps. The structure of the design is simulated and analyzed. The efficiency of the proposed meta-absorber design is investigated, and simulation results reveal that it achieves near-perfect absorption at 109.08 THz and 94.85 THz, with absorbing rates of 99.8% and 96.75%, respectively. A microwave CPC metasurface is also created and simulated. The simulation results show that the structure performs as a near-perfect cross-converter over a large frequency range (9 GHz to 15 GHz) for both the vertical and horizontal incidence polarizations. The change in reaction is steady up to 35° incidence angle. More than 99% PCR is achieved across the entire band (FBW 50%). The design development necessary to achieve these goals has been completed gradually. Furthermore, surface current distribution is used to gain a better understanding of the EM process that causes cross-polarization conversion. Lastly, a comparison with other related CPC metasurface works is provided.

REFERENCES

[1] Mulla, B. and C. Sabah, "Perfect metamaterial absorber design for solar cell applications," *Waves in Random and Complex Media*, Vol. 25, No. 3, 382–392, 2015.

[2] Bagmanci, M., M. Karaaslan, E. Unal, O. Akgol, M. Bakir, and C. Sabah, "Solar energy harvesting with ultra-broadband metamaterial absorber," *International Journal of Modern Physics B*, Vol. 33, No. 8, 1950056, 2019.

[3] Rufangura, P. and C. Sabah, "Wide-band polarization independent perfect metamaterial absorber based on concentric rings topology for solar cells application," *Journal of Alloys and Compounds*, Vol. 680, 473–479, 2016.

[4] Hamdy, H., G. Y. Abdel-Latif, M. El-Agamy, H. A. El-Mikati, M. F. O. Hameed, and S. S. A. Obayya, "Wavelength-selective metamaterial absorber based on 2D split rhombus grating for thermophotovoltic solar cell," *Optical and Quantum Electronics*, Vol. 54, No. 2, 117, 2022.

[5] Dincer, F., O. Akgol, M. Karaaslan, E. Unal, and C. Sabah, "Polarization angle independent perfect metamaterial absorbers for solar cell applications in the microwave, infrared, and visible regime," *Progress In Electromagnetics Research*, Vol. 144, 93–101, 2014.

[6] Li, J., Y. Chen, and Y. Liu, "Mathematical simulation of metamaterial solar cells," *Advances in Applied Mathematics and Mechanics*, Vol. 3, No. 6, 702–715, 2011.

[7] Herold, V. D. J., B. Antony, N. N. Teja, and V. Gandikota, "Wide band metamaterial absorber for gallium arsenide GaAs solar cells," in *2021 3rd International Conference on Signal Processing and Communication (ICPSC)*, 578–580, Coimbatore, India, 2021.

[8] Zhang, Y., Z. Yi, X. Wang, P. Chu, W. Yao, Z. Zhou, S. Cheng, Z. Liu, P. Wu, M. Pan, and Y. Yi, "Dual band visible metamaterial absorbers based on four identical ring patches," *Physica E: Low-dimensional Systems and Nanostructures*, Vol. 127, 114526, 2021.

[9] Yu, J., T. Lang, and H. Chen, "All-metal terahertz metamaterial absorber and refractive index sensing performance," in *Photonics*, Vol. 8, No. 5, 164, 2021.

[10] Tao, H., C. M. Bingham, D. Pilon, K. Fan, A. C. Strikwerda, D. Shrekenhamer, W. J. Padilla, X. Zhang, and R. D. Averitt, "A dual band terahertz metamaterial absorber," *Journal of Physics D: Applied Physics*, Vol. 43, No. 22, 225102, 2010.

[11] Cho, A., "Voilà! Cloak of invisibility unveiled," *Science*, Vol. 314, No. 5798, 403, 2006.

[12] Veselago, V. G., "The electrodynamics of substances with simultaneously negative values of ε and μ," *Soviet Physics Uspekhi*, Vol. 10, No. 4, 509–514, 1968.

[13] Fang, N., H. Lee, C. Sun, and X. Zhang, "Sub-diffraction-limited optical imaging with a silver superlens," *Science*, Vol. 308, No. 5721, 534–537, 2005.

[14] Berland, B., "Photovoltaic technologies beyond the horizon: Optical rectenna solar cell," National Renewable Energy Laboratory (NREL), 2003.

[15] Sabaawi, A. M. A., C. C. Tsimenidis, and B. S. Sharif, "Infra-red nano-antennas for solar energy collection," in *2011 Loughborough Antennas & Propagation Conference*, 1–4, Loughborough, UK, 2011.

[16] Bozzetti, M., G. de Candia, M. Gallo, O. Losito, L. Mescia, and F. Prudenzano, "Analysis and design of a solar rectenna," in *2010 IEEE International Symposium on Industrial Electronics*, Bari, Italy, 2010.

[17] Zhang, P., G. Chen, Z. Hou, Y. Zhang, J. Shen, C. Li, M. Zhao, Z. Gao, Z. Li, and T. Tang, "Ultra-broadband tunable terahertz metamaterial absorber based on double-layer vanadium dioxide square ring arrays," *Micromachines*, Vol. 13, No. 5, 669, 2022.

[18] Ustunsoy, M. P. and C. Sabah, "Dual-band high-frequency metamaterial absorber based on patch resonator for solar cell applications and its enhancement with graphene layers," *Journal of Alloys and Compounds*, Vol. 687, 514–520, 2016.

[19] Tang, J., Z. Xiao, and K. Xu, "Ultra-thin metamaterial absorber with extremely bandwidth for solar cell and sensing applications in visible region," *Optical Materials*, Vol. 60, 142–147, 2016.

[20] Montaser, A. M., "Design of multiband PIFA with low SAR value for all commercial mobile communication bands," *International Journal of RF and Microwave Computer-Aided Engineering*, Vol. 25, No. 3, 194–201, 2015.

[21] El Dein, A. Z., A. B. Abdel-Rahman, R. E. Fat-Helbary, and A. M. Montaser, "Tunable-compact bandstop defected ground structure (DGS) with lumped element," in *2010 7th International Multi-Conference on Systems, Signals and Devices*, 1–3, Amman, Jordan, 2010.

[22] Montaser, A. M., K. R. Mahmoud, A. B. Abdel-Rahman, and H. A. Elmikati, "Design Bluetooth and notched-UWB E-shape antenna using optimization techniques," *Progress In Electromagnetics Research B*, Vol. 47, 279–295, 2013.

[23] Mahmoud, K. R., A. Baz, W. Alhakami, H. Alhakami, and A. M. Montaser, "The performance of circularly polarized phased subarray antennas for 5G laptop devices investigating the radiation effects," *Progress In Electromagnetics Research C*, Vol. 110, 267–283, 2021.

[24] Ghattas, A. S. W., A. A. R. Saad, and E. E. M. Khaled, "Compact patch antenna array for 60 GHz millimeter-wave broadband applications," *Wireless Personal Communications*, Vol. 114, No. 4, 2821–2839, 2020.

[25] Rufangura, P. and C. Sabah, "Design and characterization of a dual-band perfect metamaterial absorber for solar cell applications," *Journal of Alloys and Compounds*, Vol. 671, 43–50, 2016.

[26] Akbari, M., M. Farahani, A.-R. Sebak, and T. A. Denidni, "Ka-band linear to circular polarization converter based on multilayer slab with broadband performance," *IEEE Access*, Vol. 5, 17 927–17 937, 2017.

[27] Akbari, M., H. A. Ghalyon, M. Farahani, A.-R. Sebak, and T. A. Denidni, "Spatially decoupling of CP antennas based on FSS for 30-GHz MIMO systems," *IEEE Access*, Vol. 5, 6527–6537, 2017.

[28] Akbari, M., S. Gupta, M. Farahani, A. R. Sebak, and T. A. Denidni, "Gain enhancement of circularly polarized dielectric resonator antenna based on FSS superstrate for MMW applications," *IEEE Transactions on Antennas and Propagation*, Vol. 64, No. 12, 5542–5546, 2016.

[29] Moghadam, M. S. J., M. Akbari, F. Samadi, and A.-R. Sebak, "Wideband cross polarization rotation based on reflective anisotropic surfaces," *IEEE Access*, Vol. 6, 15 919–15 925, 2018.

[30] Yu, N., P. Genevet, F. Aieta, M. A. Kats, R. Blanchard, G. Aoust, J.-P. Tetienne, Z. Gaburro, and F. Capasso, "Flat optics: Controlling wavefronts with optical antenna metasurfaces," *IEEE Journal of Selected Topics in Quantum Electronics*, Vol. 19, No. 3, 4700423, 2013.

[31] Grady, N. K., J. E. Heyes, D. R. Chowdhury, Y. Zeng, M. T. Reiten, A. K. Azad, A. J. Taylor, D. A. R. Dalvit, and H.-T. Chen, "Terahertz metamaterials for linear polarization conversion and anomalous refraction," *Science*, Vol. 340, No. 6138, 1304–1307, 2013.

[32] Li, G., M. Kang, S. Chen, S. Zhang, E. Y.-B. Pun, K. W. Cheah, and J. Li, "Spin-enabled plasmonic metasurfaces for manipulating orbital angular momentum of light," *Nano Letters*, Vol. 13, No. 9, 4148–4151, 2013.

[33] Yang, Y., W. Wang, P. Moitra, I. I. Kravchenko, D. P. Briggs, and J. Valentine, "Dielectric meta-reflectarray for broadband linear polarization conversion and optical vortex generation," *Nano Letters*, Vol. 14, No. 3, 1394–1399, 2014.

[34] Chen, H.-Y., J.-F. Wang, H. Ma, S.-B. Qu, J.-Q. Zhang, Z. Xu, and A.-X. Zhang, "Broadband perfect polarization conversion metasurfaces," *Chinese Physics B*, Vol. 24, No. 1, 014201, 2015.

[35] Grady, N. K., J. E. Heyes, D. R. Chowdhury, Y. Zeng, M. T. Reiten, A. K. Azad, A. J. Taylor, D. A. R. Dalvit, and H.-T. Chen, "Terahertz metamaterials for linear polarization conversion and anomalous refraction," *Science*, Vol. 340, No. 6138, 1304–1307, 2013.

[36] Sun, W., Q. He, J. Hao, and L. Zhou, "A transparent metamaterial to manipulate electromagnetic wave polarizations," *Optics Letters*, Vol. 36, No. 6, 927–929, 2011.

[37] Ma, H. F., G. Z. Wang, G. S. Kong, and T. J. Cui, "Broadband circular and linear polarization conversions realized by thin birefringent reflective metasurfaces," *Optical Materials Express*, Vol. 4, No. 8, 1717–1724, 2014.

[38] Zheng, Q., C. Guo, H. Li, and J. Ding, "Wideband and high efficiency reflective polarization rotator based on metasurface," *Journal of Electromagnetic Waves and Applications*, Vol. 32, No. 3, 265–273, 2018.

[39] Khan, M. I., Q. Fraz, and F. A. Tahir, "Ultra-wideband cross polarization conversion metasurface insensitive to incidence angle," *Journal of Applied Physics*, Vol. 121, No. 4, 045103, 2017.

[40] Zhao, Y. and A. Alù, "Tailoring the dispersion of plasmonic nanorods to realize broadband optical meta-waveplates," *Nano Letters*, Vol. 13, No. 3, 1086–1091, 2013.

[41] Sieber, P. E. and D. H. Werner, "Reconfigurable broadband infrared circularly polarizing reflectors based on phase changing birefringent metasurfaces," *Optics Express*, Vol. 21, No. 1, 1087–1100, 2013.

[42] Grady, N. K., J. E. Heyes, D. R. Chowdhury, Y. Zeng, M. T. Reiten, A. K. Azad, A. J. Taylor, D. A. R. Dalvit, and H.-T. Chen, "Terahertz metamaterials for linear polarization conversion and anomalous refraction," *Science*, Vol. 340, No. 6138, 1304–1307, 2013.

[43] Wu, L., M. Zhang, B. Zhu, J. Zhao, T. Jiang, and Y. Feng, "Dual-band asymmetric electromagnetic wave transmission for dual polarizations in chiral metamaterial structure," *Applied Physics B*, Vol. 117, 527–531, 2014.

[44] Zhu, H. L., S. W. Cheung, K. L. Chung, and T. I. Yuk, "Linear-to-circular polarization conversion using metasurface," *IEEE Transactions on Antennas and Propagation*, Vol. 61, No. 9, 4615–4623, 2013.

[45] Kundu, D., A. Mohan, and A. Chakrabarty, "Ultrathin high-efficiency X-band reflective polarization converter using sunken double arrowhead metasurface," in *2016 Asia-Pacific Microwave Conference (APMC)*, 1–4, New Delhi, India, 2016.

[46] Khan, M. I., F. A. Tahir, and R. Saleem, "An angularly stable tri-band reflective cross-polarization conversion anisotropic metasurface," in *2017 Progress In Electromagnetics Research Symposium — Fall (PIERS — FALL)*, 1735–1737, Singapore, Nov. 2017.

[47] Rashid, A., M. Murtaza, S. A. A. Zaidi, H. Zaki, and F. A. Tahir, "A single-layer, wideband and angularly stable metasurface based polarization converter for linear-to-linear cross-polarization conversion," *PLOS One*, Vol. 18, No. 1, e0280469, 2023.

[48] Pandey, A. and S. B. Rana, "Review of metamaterials, types and design approaches," *An International Journal of Engineering Sciences*, Vol. 17, 359–363, 2016.